The mitogenome of Norway spruce and a reappraisal of mitochondrial recombination in plants

Alexis R. Sullivan[1]
Yrin Eldfjell[2]
Bastian Schiffthaler[3]
Nicolas Delhomme[4]
Torben Asp[5]
Kim H. Hebelstrup[5]
Olivier Keech[3]
Lisa Öberg[6]
Ian Max Møller[5]
Lars Arvestad[2]
Nathaniel R. Street[3]
Xiao-Ru Wang[1]

1 – Umeå Plant Science Center, Department of Ecology and Environmental Science, Umeå University, Umeå, Sweden

2 – Department of Mathematics, Swedish e-Science Research Centre, Science for Life Laboratory, Stockholm University, Stockholm, Sweden

3 – Umeå Plant Science Center, Department of Plant Physiology, Umeå University, Umeå, Sweden

4 – Umeå Plant Science Center, Department of Forest Genetics and Plant Physiology, Swedish University of Agricultural Sciences, Umeå, Sweden

5 – Department of Molecular Biology and Genetics, Aarhus University, Slagelse, Denmark

6 – oldTjikko Photo Art & Science, Handöl 544 Fjällforsa, SE-83015 Duved, Sweden

Corresponding author: Alexis R. Sullivan alexis.sullivan@umu.se

Abstract

Plant mitogenomes can be difficult to assemble because they are highly structurally dynamic and prone to intergenomic DNA transfers, leading to the unusual situation where an organelle genome is far outnumbered by its nuclear counterparts. As a result, comparative mitogenome studies are in their infancy and some key aspects of genome evolution are still known mainly from pre-genome, qualitative methods. To help address these limitations, we combined machine learning and *in silico* enrichment of mitochondrial-like reads to assemble the bacterial-sized mitogenome of Norway spruce (Pinaceae: *Picea abies*) from whole genome long-read shotgun sequencing reads. We conducted comparative analyses of repeat abundance, intergenomic transfers, substitution and rearrangement rates, and estimated repeat-by-repeat homologous recombination rates. Prompted by our discovery of highly recombinogenic small repeats in *P. abies*, we assessed the genomic support for the prevailing hypothesis that intramolecular recombination is predominantly driven by repeat length, with larger repeats facilitating DNA exchange more readily. Overall, we found mixed support for this view: recombination dynamics were heterogeneous across vascular plants and highly active small repeats (*ca*. 200 bp) were present in about a third of studied mitogenomes. As in previous studies, we did not observe any robust relationships among commonly-studied genome attributes, but we identify variation in recombination rates as a underinvestigated source of plant mitogenome diversity.

Key words: mitogenome, repeats, recombination, rearrangement rates, structural variation

Introduction

Mitochondria share an α-proteobacterium ancestor, a conserved core proteome, and an almost universal function as the site of cellular energy production (Gray 2014). Despite the broad similarity of mitochondria across eukaryotes, the vestigial mitogenome is remarkably diverse in size, content, and architecture (Burger et al. 2003). Nowhere is this heterogeneity showcased more clearly than in plants: closely-related mitogenomes can vary 100-fold or more in size (Sloan et al. 2012), substitution rates (Cho et al. 2004), and rearrangement rates (Cole et al. 2018). Gene repertoires are fluid due to recurrent horizontal (Rice et al. 2013) and intergenomic transfers (Cho et al. 2004). Multichromosomal architectures (Alverson, Rice, et al. 2011; Sloan et al. 2012) have also been reported from the relatively few sequenced plant mitogenomes. Underlying the evolutionary dynamism of plants appears to be the evolution of pervasive homologous recombination (Palmer & Herbon 1988; Gray et al. 1999).

Recombination is the predominant mode of double-strand break repair in plant mitogenomes (Maréchal & Brisson 2010; Gualberto & Newton 2017). In contrast, animal mitogenomes tend to use non-homologous end joining pathways or simply degrade damaged molecules (Alexeyev et al. 2013). Recombination can preserve sequence identity, but reliance on this pathway may lead to unsuppressed intramolecular recombination at dispersed repeats (Maréchal & Brisson 2010). While these differences in repair pathways likely contribute to the broad scale mitogenome differences among eukaryotic kingdoms, the importance of recombination and other mechanisms in generating the myriad evolutionary trajectories followed by plants are unclear. Our limited understanding stems, in part, from the few available assembled mitogenomes.

While sequencing plant genomes is routine, only one mitogenome is published for every four nuclear genomes (NCBI Genome Resource; accessed March 11, 2019). Often, mitogenome assembly requires isolating DNA directly from intact mitochondria because frequent intergenomic transfers (e.g. Alverson, Rice, et al. 2011), the rapid decay of intergenic sequence homology (Guo et al. 2016), and the unclear physical organization of the mitogenome (Sloan 2013) can preclude identifying mitochondrial sequences from whole genome read data (e.g. Nystedt et al. 2013). Strategies to identify mitogenomic scaffolds using GC-content and genome copy number can be effective (e.g. Naito et al. 2013), but this simple strategy becomes prone to false positives and low recovery rates with increasingly large, complex genomes (Eldfjell 2018).

We used machine learning to assemble the bacterial-sized mitogenome of a coniferous forest tree, Norway spruce (Pinaceae: *Picea abies*), from whole-genome shotgun sequencing reads. The *P. abies* mitogenome helps to fill a phylogenetic gap in comparative analyses, and to that end we analyzed gene repertoires; sources of genome size heterogeneity; intraspecific variation; and mutation, recombination, and rearrangement rates. Prompted by the detection of highly recombinogenic small repeats in *P. abies*, we reevaluated published recombination rates in seed plants. Despite early recognition of recombination as a factor in generating the diversity of eukaryotic mitogenomes (Palmer & Herbon 1988; Gray et al. 1999), surprisingly little attention has been given to recombinational dynamics as a source of mitogenomic diversity within plants. As in previous studies, we found no obvious relationship between mitogenome traits and potential mechanisms – for example, genome size and DNA import – but the role of recombination as a driver of mitogenomic diversity within plants mertis further scrutiny.

Results and Discussion

Machine learning improves mitogenome assembly

We combined machine learning, *in silico* enrichment of long sequencing reads, and assembly reconciliation to produce a highly contiguous *P. abies* draft mitogenome. First, we trained a support vector machine (SVM) to identify mitogenome-like scaffolds from the *P. abies* v. 1.0 assembly (Nystedt et al. 2013). Of these, the SVM identified 301 scaffolds totaling 4.69 Mb as mitochondrial in origin. While SVMs are more powerful than coverage *vs.* GC-content plots (Eldfjell 2018), recall and false discovery rates (FDR) estimated from cross-validation indicate the SVM classification alone would be insufficient to robustly identify mitochondrial sequences in the *P. abies* assembly; recall ranged from 0.53 to 0.92 and the FDR from 0.13 to 0.22 with varying test-to-training ratios (Table S1). Additional post-classification filters may improve the accuracy of SVM, but our goal was only to identify a set of scaffolds to use as ‘bait’ to enrich Pacific Biosciences (PacBio) Sequel® whole genome reads through kmer matching. We reasoned that the long average length (12,004 bp) of the matched reads would enable us to recover a greater proportion of the mitogenome while allowing removal of dubious contigs post-assembly.

Table 1. Summary statistics for assemblies of Pacific Biosciences Sequel® reads enriched *in silico* for mitochondrial-like kmers. 'Raw' refers to the full contig output produced by each assembler. Upgraded assemblies have been processed with FinisherSC. High-confidence assemblies contain only contigs with at least one conserved mitochondrial gene. N50 and L50 are calculated from contig lengths.

Assembler	#Contigs	N50 (Mb)	L50	Longest contig (Mb)	Assembly size (Mb)
canu					
raw	383	0.06	18	1.10	10.25
upgraded	276	0.32	4	2.36	9.76
high conf.	4	1.28	2	2.56	5.29
MECAT					
raw	104	0.43	5	2.29	9.24
upgraded	95	0.43	5	2.29	9.22
high conf.	6	0.70	2	2.29	5.10
SMARTdenovo					
raw	59	0.76	2	3.60	7.31
upgraded	55	0.76	2	3.60	7.32
high-conf.	4	3.60	1	3.60	5.13
final draft	**4**	**3.42**	**1**	**3.42**	**4.90**

We assembled the SVM-enriched PacBio reads using three assemblers selected based on their prior performance (Jayakumar & Sakakibara 2017; Giordano et al. 2017). The most contiguous results per assembler are summarized in Table 1. Upgrading the initial assemblies with unused overlap information in the corrected PacBio reads with FinisherSC (Lam et al. 2015) only appreciably improved the N50 of the canu (Koren et al. 2017) assembly (Table 1). Despite initial differences in size and contiguity, the assemblies were similar when considering only contigs with at least one of the 41 mitochondrial protein-coding genes conserved in *Gingko* and *Cycas*, which we term high-confidence assemblies (Table 1). Finally, reconciliation using the Contig Integrator for Sequence Assembly (CISA) pipeline (Lin & Liao 2013) produced a final draft assembly measuring 4.9 Mb over four contigs with a mean depth of coverage of 284x.

Genome annotation

General features of the *P. abies* mitogenome are summarized in Table 2. All 41 protein-coding genes inferred to be present in the last common ancestor of angiosperms are also found in *P. abies* and, after re-annotation, also in *P. glauca* and *Pinus taeda.* This pattern of conservation in Pinaceae is consistent with the early-diverging gymnosperms *Gingko* and *Cycas*, which may

suggest a less dynamic gene repertoire than in angiosperms, although *Welwitschia* has undergone angiosperm-like gene losses (Guo et al. 2016). In addition, the *P. abies* mitogenome has also acquired complete copies of four plastid genes, *psaB*, *psbH*, *psbN*, and *psbT*, which brings the total described gene count to 45. We also identified 20 transcribed open-reading frames: 14 had uniquely mapping transcripts of ≥ 99% coverage and identity (high confidence), two were of medium confidence where either identity or coverage was < 99% but > 97%, and four low confidence genes had less than 97% support (Table S2). Intron and tRNA content were similar in *P. abies* and *P. glauca* (Jackman et al. 2015), but both have apparently undergone losses compared to the other gymnosperms, including the Pinaceae conifer *Pinus taeda*.

The repetitive fraction of the *P. abies* mitogenome is larger than the entire mitogenome of most plants (Table 2; Table S3). Relative to genome size, however, repeat content in *P. abies* is unremarkable. Dispersed repeats in 82 angiosperms comprised 14% of the mitogenome on average (Dong et al. 2018), identical to the proportion in *P. abies* (Table 2). However, dispersed repeats in *P. abies* tended to be about half the size of a typical tracheophyte, at 312 bp *vs.* the 641 bp average (Wynn & Christensen 2019), indicating a relative enrichment of smaller repeats (Fig. S1). At the same time, *P. abies* also had eight pairs of repeats ≥ 10 Kb, more than all but two of the 79 land plants analyzed by Wynn & Christensen (2019).

Table 2. Characteristics of the *Picea abies* mitochondrial genome.

Genome	
Size (Mb)	*ca.* 4.90
GC content	44.7%
Annotation	
Repeat content	15.15%
Direct and inverted	14.25%
Tandem	1.12%
Nuclear-mitochondrial DNA	28.89%
Transposable elements	7.72%
Plastid-derived DNA	0.34%
Genes	1.0%
Protein coding genes	45
Hypothetical proteins high/medium/low confidence	14/2/4
tRNAs	17
rRNAs	3

Extraordinary mitogenome size heterogeneity among plants has long been recognized (Ward et al. 1981), but the sources are inconsistent among species. We analyzed intergenomic transfers and the proliferation of repetitive sequences as potential causes of genome size variation in gymnosperms. Transfer of plastid DNA made a negligible contribution to the genome size of the three Pinaceae conifers (Table 3), in contrast to some angiosperms, such as cucurbits (Alverson, Rice, et al. 2011; Alverson et al. 2010). Similarly, no relationship between

genome size and repeat proliferation was evident: the 410 kb *Cycas* mitogenome was proportionally the most repetitive (Chaw et al. 2008), and relative repeat content was similar in *Picea* and *Ginkgo* despite their > 10x size differences (Table 3). An ambiguous – or absent – correlation between genome size and repeat proliferation was also observed in *Silene* (Sloan et al. 2012), whereas repeat content in cucurbits scaled with genome size (Alverson et al. 2010; Alverson, Rice, et al. 2011; Rodríguez-Moreno et al. 2011).

Table 3. Potential sources of mitogenome size variation among gymnosperms. Dispersed repeats include inverted and direct repeats ≥ 50 bp and with ≥ 80% identity. Nuclear-mitochondrial DNA are shared sequences with no direction of transfer inferred. Transposable elements comprises long-terminal repeats (LTR) and non-LTR retrotransposons. Numbers in parenthesis indicate percent coverage of the mitogenome.

	Cycas	*Ginkgo*	*Picea abies*	*Picea glauca*	*Pinus taeda*	*Welwitschia*
Genome size (Mb)	0.41	0.35	4.90	5.20†	1.19	0.98
Plastid-derived DNA (kb)	18 (4)	0 (0)	17 (0)	18 (0)	3 (0)	9 (9)
Dispersed repeats (kb)	109 (26)	51 (15)	699 (14)	885 (17)	83 (7)	42 (4)
Nuclear-mtDNA (Mb)	-	0.35 (100)	1.40 (29)	2.29 (44)	0.60 (50)	-
Transposable elements (kb)	6 (1)	3 (1)	482 (10)	386 (7)	129 (10)	15 (2)

†Gene-containing scaffolds extracted from the putative 5.9 Mb assembly.

Interpreting shared nuclear-mitochondrial content is difficult because 1) the nuclear genomes of *Cycas* and *Welwitschia* are not sequenced; 2) the direction of transfer can rarely be determined with confidence under the simplest circumstances (Alverson et al. 2010); and 3) the *Cycas* and *Ginkgo* mitogenomes are highly conserved, which implies that any import from the nucleus predate their divergence *ca*. 354 My ago (Lu et al. 2014) and may no longer be detectable in either nuclear genome (Guo et al. 2016). Therefore, it is unsurprising that the four species with nuclear reference genomes show an equivocal relationship between mitogenome size and shared nuclear-mitochondrial sequence (Table 3). Remnants of nuclear transposable elements (TEs) can potentially act as markers of sequence import because they have an unambiguous origin and generally do not proliferate after transfer (Knoop et al. 1996; Goremykin et al. 2012). All three Pinaceae species showed an increase of TE remnants, but relative content was similar among the two *Picea* species and the 4-fold smaller *P. taeda* mitogenome (Table 3). Similarly, *Welwitschia* was relatively depauperate in TE elements, despite its relatively large mitogenome size (Table 3). Increased sampling may help to clarify this ambiguous relationship between TE import and genome size, and but a similarly unclear

relationship has also been reported among angiosperms (Alverson et al. 2010; Alverson, Rice, et al. 2011; Rodríguez-Moreno et al. 2011, Goremykin et al. 2012). Overall, gymnosperms tend to reinforce observations in angiosperms: repeat proliferation and DNA imports do not clearly scale with mitogenome size (Alverson, Rice, et al. 2011; Sloan et al. 2012; Dong et al. 2018; Alverson et al. 2010).

Abundant repeat-mediated recombination at small repeats

Homologous intermolecular recombination is used to repair double-stranded breaks and recover stalled replication forks (Maréchal & Brisson 2010). In many plants, intramolecular recombination also occurs at dispersed repeats and results in an individual harboring alternative genome configurations (AGCs) that differ in structure but are identical in sequence. Intramolecular recombination dynamics range from completely inert (Alverson, Rice, et al. 2011; Dong et al. 2018) to astonishingly friable (Skippington et al. 2015), yet recombination rates are not widely estimated (see next section). Recombination resulting in DNA exchange produces AGCs that are directly observable in a pool of single molecule sequencing reads (e.g. Dong et al. 2018; Wang et al. 2018). This allowed us to estimate the AGC frequency associated with each pair of inverted repeats in the *P. abies* mitogenome, which provides a quantitative estimate of recombination rates.

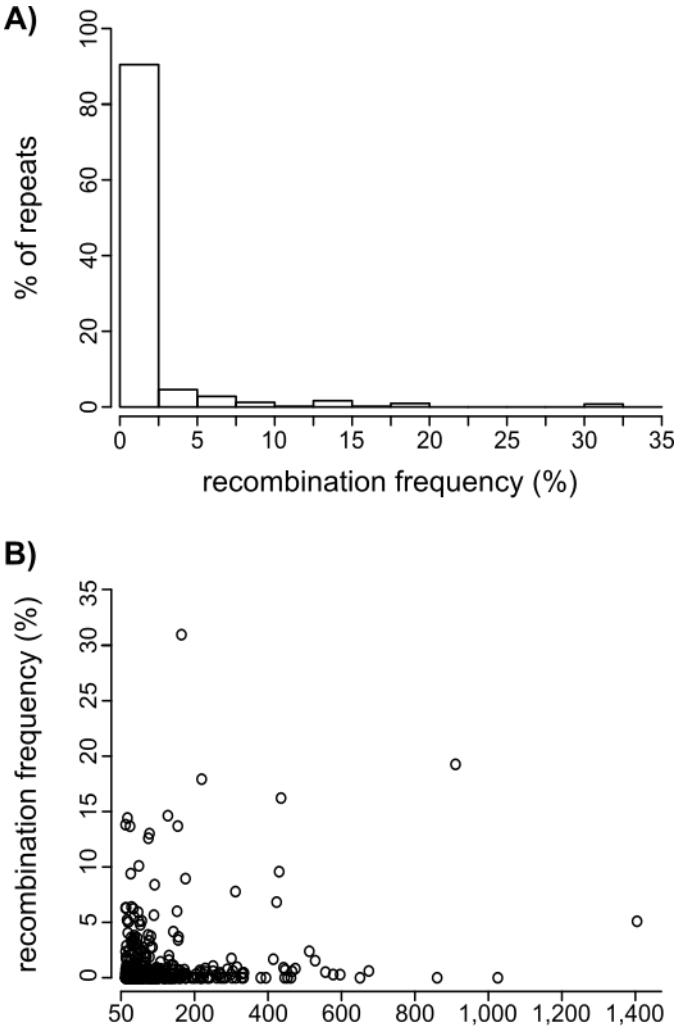

Figure 1. Recombination frequency at inverted repeats ≥ 50 bp with ≥ 80% pairwise identity as inferred from long reads mapping to expected recombination products (alternative genome configurations; AGCs). A) Most repeat pairs have little or no evidence of recombination, but a minority are highly active. B) Repeat length explains very little of the variation in recombination frequency.

Genome rearrangements consistent with the products of intramolecular recombination

(i.e., AGCs) comprised *ca*. 1% of the pool of mitochondrial sequencing reads. Half of the 598 repeats showed no evidence of recombination, but AGC frequency averaged 2% at recombinogenic repeats (Fig. 1A; Table S4). Recombination was asymmetric in most cases, a result consistent with the repair of stalled replication forks through break-induced replication (Table S4; Maréchal & Brisson 2010). AGC abundance reached a maximum of 32% at a 186 bp repeat, with the two possible isomers comprising 12% and 20% of the reads, respectively. Surprisingly, the most recombinogenic repeats (AGCs ≥ 10%) ranged in size from 50 bp, the minimum size evaluated, to 948 bp (Fig. 1A; Table S4). Overall, we found a negligible correlation between repeat length and AGC frequency (Fig. 1B; $r^2 = 0.03$, $p < 0.001$), in contrast to some well-characterized examples (e.g. Mower, Floro, et al. 2012; Skippington et al. 2015; Guo et al. 2016) and contrary to the general expectation that, in the absence of other factors, recombination should scale positively with repeat length (Arrieta-Montiel & Mackenzie 2011).

A reappraisal of intramolecular mitogenome recombination

Plant mitogenomes are widely cited to undergo frequent, reciprocal recombination at large repeats and only rarely elsewhere based on the results of seminal pre-genomic (Lonsdale et al. 1984; Palmer & Shields 1984; Arrieta-Montiel & Mackenzie 2011). As our results suggest *P. abies* deviates from this pattern, we tested if this canonical model of mitogenome evolution is still supported by modern sequencing data. We searched the *ca*. 200 published tracheophyte mitogenomes and discarded those with insufficient read coverage to identify AGCs occurring at a minimum 1.6% frequency. Most of the remaining studies did not analyze repeat-by-repeat dynamics, but 18 mitogenome analyses representing ferns, gymnosperms, and four major angiosperm lineages met our criteria.

Table 4. Recombination patterns by repeat size class inferred from high-throughput sequencing mapping rates in 18 vascular plants. 'Proportion active' refers to the fraction of repeats producing alternative genome configurations (AGCs) inferred to be the product of recombination in frequencies ≥ 1.6% of the parent molecule. 'Max AGC' denotes the maximum frequency obtained by any isomer in the given repeat size class. Missing data because repeats of that size class do not exist in a given genome is listed as 'na', whereas '-' indicates missing data due to study limitations.

Species	repeats ≥ 1,000 bp		repeats < 1,000 bp		Study
	Proportion Active	Max AGC %	Proportion Active	Max AGC %	
Chrysanthemum nankingense	na	na	0.17	4	Wang et al. 2018
Cucumis sativus	1	50	0.08	5	Alverson, Rice, et al. 2011
Daucus carota	0.25	50	0.00	0	Iorizzo et al. 2012
Eucalyptus grandis	0.40	31	0.04	23	Pinard et al. 2019
Ginkgo biloba	1.00	50	0.00	0	Guo et al. 2016
Mimulus guttatus	1.00	50	0.38*	50	Mower, Floro, et al. 2012
Monsonia ciliata	-	-	0.00	0	Cole et al. 2018
Monsonia herrei	na	na	0.00	0	Cole et al. 2018
Nymphaea colorata	0.00	8	0.00	0	Dong et al. 2018
Ophioglossum californicum	0.50	25	0.00	0	Guo et al. 2017
Picea abies†	0.50	6	0.13	31	this study
Psilotum nudum	0.00	0	0.03	2	Guo et al. 2017
Silene conica	0.48	13	0.06	15	Sloan et al. 2012
Silene noctiflora	0.78	10	0.00	0	Sloan, Alverson, et al. 2012
Silene vulgaris	1.00	50	0.14	10	Sloan, Alverson, et al. 2012
Vigna angularis	1.00	33	0.26	24	Naito et al. 2013
Viscum scurruloideum	-	-	0.66	50	Skippington et al. 2015
Welwitschia mirabilis	na	na	0.00	0	Guo et al. 2016

† only inverted repeats analyzed
* minimum detection threshold is *ca.* 4%, thus this proportion is underestimated

Recombination patterns across tracheophytes provided mixed support for the canonical model of mitogenome evolution (Table 4, Table S5). As predicted, large repeats tended to be more active than their smaller counterparts (Table 4). However, AGC abundances were not at equilibrium with their reciprocal configurations in most species (Table 4), indicating a lower recombination rate than anticipated from Southern blots (Maréchal & Brisson 2010). Although small repeats were overall less recombinogenic, active small repeats produced AGCs at similar frequencies as their larger counterparts in 33% of species, including *P. abies* (Table 4). All species with active small repeats except for *Silene conica* showed high AGC frequencies at repeats measuring just *ca*. 200 bp in length (Sloan et al. 2012; Mower, Floro, et al. 2012; Naito et

al. 2013; Skippington et al. 2015; Pinard et al. 2019). References to recombination rates are often necessarily vague, but the 10-50% AGC abundances in these species exceed any reasonable interpretation of phrases such as 'highly substoichiometric,' which are frequently used to describe the activity of small repeats (Woloszynska 2009; Arrieta-Montiel & Mackenzie 2011). Together, these studies point to the importance of small repeats as drivers of mitogenome evolution, a long anticipated (André et al. 1992) but rarely quantified phenomenon.

Differences in the nuclear-encoded repair pathways may be the mechanism underlying heterogeneity in recombination rates (Maréchal & Brisson 2010; Gualberto & Newton 2017). For example, *Arabidopsis* mutants for mitochondrial repair and surveillance genes recombine more readily at small repeats (Zaegel et al. 2006; Shedge et al. 2007; Miller-Messmer et al. 2012; Wallet et al. 2015). While mutations associated with these or undiscovered genes could contribute to the diversity of recombination dynamics, the results in Table 4 do not show any discernable phylogenetic signal. If nuclear-encoded repair pathways directly explain most of the observed differences in recombination dynamics, then this lack of signal implies repeated, independent evolution. Identifying factors influencing recombination rates, and in turn how – or if – their variation explains facets of genome evolution such as genome size, repeat content, and mutation rate would be aided by more widespread and consistent reporting of recombination rates.

Rampant mitogenome rearrangements in Picea

Rearrangements between the *P. abies* and *P. glauca* mitogenomes occurred an average of every 1,540 bp and blocks of synteny rarely extended beyond gene boundaries (Fig. 2). After accounting for the draft state of the genomes (Muñoz & Sankoff 2010), a parsimonious rearrangement scenario (Tesler 2002) required 1,292 events to explain the size and distribution of synteny blocks between the *Picea* species. Assuming a divergence time of approximately 15 My ago (95% CI: 10-18 My; Feng et al. 2018) results in an absolute rearrangement rate of around 71-129 rearrangements My^{-1}. This rate is similar to those observed in *Silene vulgaris* and some closely-related *Monsonia* species (Cole et al. 2018), which appear exceptionally rearranged relative to other eukaryotes. Rearrangement inference methods used here and by Cole et al. (2018) do not correct for events that have been lost due to the erosion of shared sequence over time, which should underestimate rearrangements given increasing divergence. When comparing similarly diverged mitogenomes (*ca.* 50% shared sequence) to mitigate this bias, the high

rearrangement rate in *Picea* is even clearer: 86 *vs.* an average 2.5 rearrangements My^{-1} (SD: 0.39) for four other species pairs (Table S6). Repeat content and their recombination frequencies is a probable explanation for the over 700-fold difference in rearrangement rates observed in plants (Cole et al. 2018).

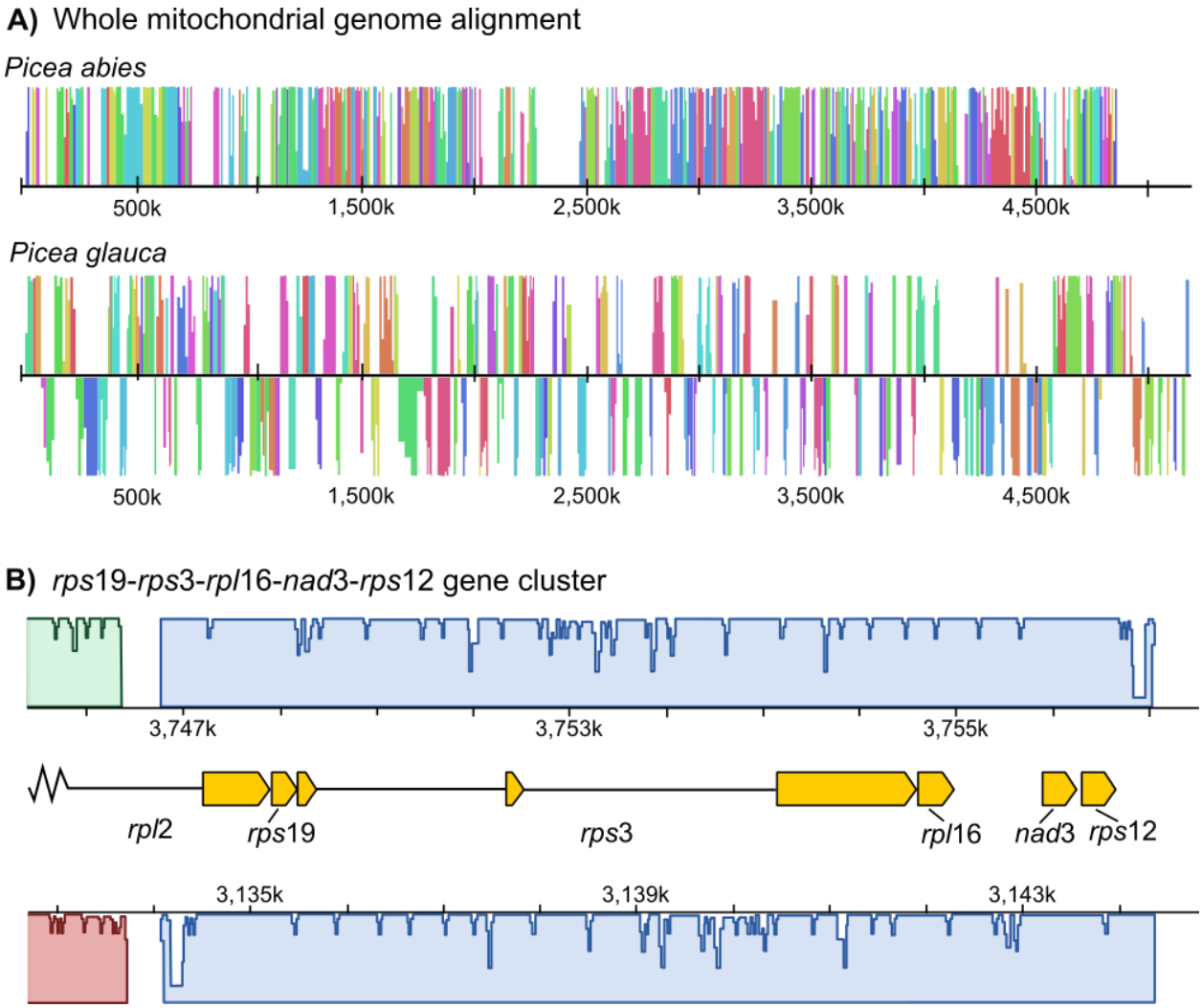

Figure 2. Mitogenomes of the two sequenced *Picea* species are extensively rearranged and collinear regions are limited to genic regions. An absolute rearrangement rate of 71-129 My^{-1} is needed to explain this level of structural divergence. A) Simplified diagram of the *P. abies-P. glauca* alignment, where colored blocks represent regions free of internal re-arrangements (locally collinear blocks; LCBs) and heights are proportional to pairwise sequence identity. LCBs below the centered line are inverted with respect to *P. abies*. White space indicates regions with no homology. Only LCBs longer than 2,000 bp are shown. B) Two gene clusters widely conserved in plant mitogenomes are also found in *Picea* within a 9 kb block, which also serves to illustrate the typical extent of synteny beyond genic regions. Gene structures are indicated by yellow boxes and introns by black lines.

Mitogenome shuffling in *Picea* is stunning in contrast to the remarkably static Pinaceae nuclear genome, where a high degree of synteny persists among genera after ≥ 140 My of

divergence (Krutovsky et al. 2004; Pelgas et al. 2006; Pavy et al. 2012). Even the nuclear genomes of Cupressaceae and Pinaceae, which last shared a common ancestor in the Carboniferous (Leslie et al. 2018), are more collinear than the *P. abies* and *P. glauca* mitogenomes (Ehrenmann et al. 2015). Despite their extensive rearrangements, two of the three gene clusters widely preserved in tracheophytes from their α-proteobacterial endosymbiont (Dong et al. 2018) were also maintained in *Picea* within the same 9 kb block: *rpl*2-*rps*19-*rps*3-*rpl*16 and *nad*3-*rps*12 (Fig. 2B). The third widely-conserved gene cluster – *rrn*5-*rrn*18 – has not been preserved in *Picea*, *Pinus taeda*, or *Welwitschia* but persisted in *Cycas* and *Ginkgo* (Guo et al. 2016), suggesting it was lost in the common ancestor of conifers and gnetophytes.

Intramolecular recombination creates AGCs that can potentially be transmitted as rearrangements (Gualberto & Newton 2017; Cole et al. 2018). However, the path from isomer to rearrangement is not straightforward because mitogenomes are subject to genetic drift within an individual and within a population (Gualberto & Newton 2017). After an AGC is produced, it must survive multiple rounds of cell division, be recruited into the germline, and persist through potentially multiple generations before the rearrangement becomes firmly established within an individual (Davila et al. 2011). Proliferation throughout the population could then occur as other polymorphisms, probably predominately through stochastic demographic forces but possibly also through natural selection (Shedge et al. 2010). Several aspects of this process are unknown, including how mitogenomes are replicated (Gualberto & Newton 2017), the timing of germline segregation (Lanfear 2018), and when, where, and under what circumstances AGCs arise. For these reasons, the relationship between recombination within individuals summarized in Table 4 and re-arrangement rates among species is unclear. For example, *Monsonia* and *Silene vulgaris* have markedly different levels of intramolecular recombination (Table 4), yet have similar interspecific rearrangement rates (Cole et al. 2018).

Sequence divergence in Picea *and among gymnosperms*

A strong dichotomy between rates of sequence and structural evolution is a well-known feature of plant mitogenomes (Palmer & Herbon 1988) and is also the dynamic found in *Picea* and other Pinaceae conifers (Fig. 3). Substitution rates across all protein-coding genes averaged 0.0023 for synonymous and 0.0012 for nonsynonymous mutations. These rates are about 1/2 of those in the plastid genome (Sullivan et al. 2017) and 1/4 of the nuclear genome (Buschiazzo et al. 2012; Chen et al. 2012). Assuming a divergence time of 10-17 My between *P. abies* and *P. glauca* (Feng et al. 2018), mitochondrial mutation rates in *Picea* fall within the lower end of absolute rates observed in angiosperms (dS = 1.53 x 10^{-10}; dN = 0.80 x 10^{-10}; Mower et al. 2007) and are slightly higher than in *Cycas* and *Ginkgo* (Guo et al. 2016). Absolute substitution rates in *Pinus*, however, are among the lowest reported in vascular plants (Richardson et al. 2013). Using divergence times from Saladin et al. (2017), rates ranged from dS = 0.12 x 10^{-10} and dN = 0.06 x 10^{-10} site/year in *Pinus taeda* to dS = 0.63 x 10^{-10} and dN = 0.34 x 10^{-10} in *Pinus strobus*. Previous work with more taxa, but fewer loci, simil(arly inferred exceptionally low mutation rates in some *Pinus* species (Wang & Wang 2014). At the other extreme, absolute dS measured *ca*. 6.0 x 10^{-10} site/year in *Welwitschia* and *Araucaria heterophylla* when assuming a divergence from Pinaceae around 342 My ago (Lu et al. 2014). Relative substitution rates were consistent with previous studies analyzing fewer genes or species (e.g. Mower et al. 2007; Guo et al. 2016) and are reported in Table S7.

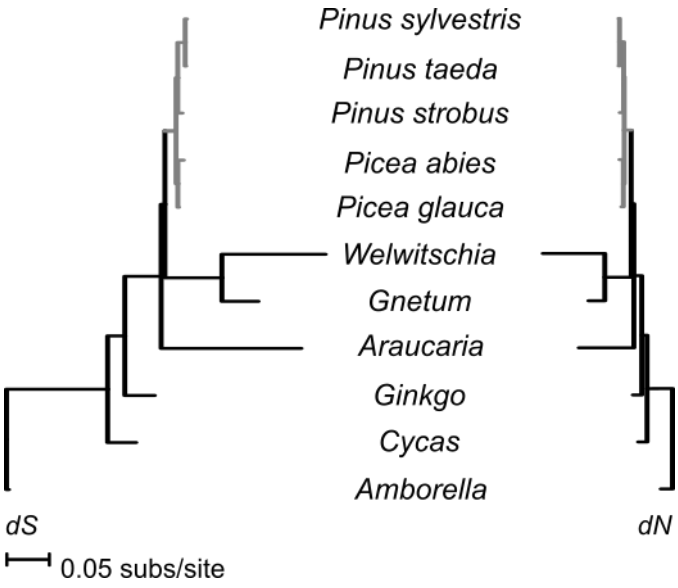

Figure 3. Mean substitution rates at synonymous (dS) and nonsynonymous (dN) sites vary 100-fold among gymnosperms. Rates within Pinaceae, in gray, are more consistent but are about 6-fold higher in *Picea* than in the 75% smaller *Pinus* mitogenomes.

Intraspecific variation

We used the PacBio Sequel® system to sequence partial mitogenomes from two isolated *P. abies* trees from the alpine tundra in central Sweden, about 400 km southwest from the reference tree. *Picea* megafossil remains in this region date to *ca*. 11,000 ^{14}C yr^{-1}, which suggests the presence of high-latitude glacial refugia in Scandinavia (Kullman 2008). Both formed small clonal groups above the modern tree line and are spatially associated with megafossils dated to 5,120 and 4,820 ^{14}C yr^{-1}, respectively, raising the possibility that these clonal groups are extremely ancient (Kullman 2001). Thus, the mitogenomes of these two trees is relevant to post-glacial recolonization history and to the study of mitochondrial repair and recombination dynamics in long-lived organisms. In total, we recovered 499,180 and 553,660 bp, respectively, of which 82,443 was shared between the two trees. Nine variant sites were shared by the two trees, and the remaining sites were only sequenced in a single tree. In contrast, 58 structural variations were found between these putatively ancient trees and the reference individual: 29 insertions, 17 deletions, 13 translocations, nine duplications, and seven inversions. While more data is needed to address ecological and molecular hypotheses, these sequences demonstrate the feasibility of later intraspecific mitogenome studies in *Picea*.

Conclusion

Plant mitogenomes are highly variable in size, repeat and gene content, and mutation and rearrangement rates. The underlying processes generating this heterogeneity are largely unclear: for each mitogenome supporting a given mechanistic hypothesis, another suggests the opposite, such as in the relationship between mutation rate and genome size (cf. Sloan et al. 2012; Skippington et al. 2015). The *P. abies* mitogenome and our comparative analyses may lend support to the view of plant mitogenomes as highly idiosyncratic and driven mainly by rapid evolution and/or considerable genetic drift. As in previous studies, we found no clear relationship between genome size, repeat content, intergenomic transfer, or mutation rate. However, we identified recombination as an underinvestigated mechanism of plant mitogenome evolution, despite being recognized as a likely source of the differences among eukaryotes (Palmer & Herbon 1988; Gray et al. 1999). Recombination rates vary extensively among plants and small repeats (< 1,000 bp) are highly active in a third of the reported species. Recombination affects the accumulation of mutations (Maréchal & Brisson 2010), influences genome size and the efficiency of selection (Tiley & Burleigh 2015), and induces structural rearrangements

(Palmer & Herbon 1988), making this variation a potential but understudied contributor to the diversity of plant mitogenomes.

Methods

Machine learning classification of WGS scaffolds

The SVM involved three steps: 1) identification of high-quality training data, 2) training the classifier, and 3) evaluation of the model performance. To curate a reliable set of positive and negative training data from *P. abies*, we first discarded scaffolds < 500 bp and masked repetitive elements using RepeatMasker v. open-4.0.1 (Smit et al. 2013). We aligned the remaining scaffolds to a set of relatively well-annotated genomes, including *Arabidopsis thaliana* and *Populus trichocarpa* and 18 additional organelle genomes (Table S8), using blastn and tblastx in BLAST version 2.2.29+ with default parameters except for an e-value cutoff of 1e-20. Known numts (nuclear mitochondrial DNA sequences) were masked from the *Arabidopsis* assemblies. *P. abies* sequences were considered robustly assigned if they matched an annotated gene region on the subject genome and 1) the top bitscore was > 100; 2) the quotient between the top bitscore and next-best hit was > 1.2; 3) alignments spanned at least 150 bp for blastn and 100 aa for tblastx; 4) blastn and tblastx annotations were identical if both existed; and 5) at least two different reference species contained the BLAST hit. Scaffolds meeting all these criteria were then classified as mitochondrial or non-mitochondrial and as training data for the SVM classifier. This yielded 2.0 Mb and 51.1 Mb of positive and negative data, respectively, for training the SVM.

After identifying robust positive and negative training datasets, we trained the SVM classifier to distinguish between them using pre-determined features. Following previous studies (Nystedt et al. 2013; Jackman et al. 2015), we used the standardized values of the natural logarithm of mean depth of coverage, the proportion of ambiguous nucleotides (%N), and the proportion of guanine and cytosine (%GC) for each scaffold, and a kmer-based score based on the frequency of nonredundant ‘mitochondrial-like’ or ‘non-mitochondrial-like’ oligonucleotide sequences in a scaffold. We calculated probability tables for occurring kmers based on positive and negative training sequences and calculated a score for each accordingly:

$$s_c = \prod_{k=1}^{n} p_{c,kmer_k}$$

where c is the class, n is the number of kmers in the scaffold, and $p_{c,kmer_k}$ is the probability of kmer k occurring in a sequence of class c. The final kmer classifier score for each scaffold was calculated as:

$$s = \frac{\log s_{pos} - \log s_{neg}}{L}$$

where L is the scaffold length and s_{pos} and s_{neg} are the positive and negative scores as defined above. Thus, smaller scores are consistent with plastid or nuclear sequence whereas larger scores indicate a scaffold comprising more mitochondrial-like kmers. Optimal kmer size for the classifier (k = 7, here) was assessed using test and training data from *A. thaliana* and visual inspection of the receiver operating characteristic (ROC) curves. After defining these features, we used SVMlight (Joachims 1999) with a Gaussian kernel to conduct the training step and to apply the learned model to the set of *P. abies* scaffolds with length > 500 bp and coverage > 100x. Limiting the scope of the SVM to scaffolds > 500 bp and with coverage > 100x removed the vast majority of the 12 Gb assembly but 49,500 scaffolds remained to be classified.

We assessed the SVM model performance using cross-validation. The initial training data were divided randomly into nine trials varying in training subsets from 10-90%, each consisting of 100 cross-validation tests. Kmer scores, SVM training, and classification were carried out as described above. For each trial, we calculated the mean false discovery rate (FDR) and true positive recall.

Mitogenome assembly

We used the mitochondrial scaffolds identified by the SVM for *in silico* enrichment of 77 SMRT cells of PacBio Sequel® reads generated from total genomic DNA from vegetative tissue (Street et al., unpublished data) through kmer matching. We screened *ca.* 35.5 million subreads totaling 244 Gbp for 27-mer matches to any of the SVM-classified scaffolds or the *P. glauca* draft mtDNA (Jackman et al. 2015) using BBDuk v. 35.14 (http://jgi.doe.gov/data-and-tools/bb-tools). This yielded 3.23 million reads totaling 4.1 Gb, with an average read length of 12,041 bp, which were assembled using canu v. 1.7 (Koren et al. 2017), MECAT v. 1.3 (Xiao et al. 2017), and SMARTdenovo (https://github.com/ruanjue/smartdenovo). Canu was run using default parameters, except `corMaxEvidenceErate` was set to 0.15 as recommended in the manual for repetitive and GC-skewed genomes. MECAT was also run using default parameters

using a target of 45x, 55x, and 65x coverage of the longest corrected reads. For MECAT and canu, we specified a genome size of approximately 5.0 Mb, which is used to estimate the coverage of the input reads. Because SMARTdenovo does not include a preassembly read correction step, we used the 45x, 55x, and 65x corrected reads from MECAT as input and the default parameters were then used for assembly.

We selected the most contiguous assembly from each assembler for further refinement. We passed these assemblies and their constituent reads to FinisherSC to reconstruct the overlap graph and identify contigs that can be robustly merged (Lam et al. 2015). We refer to the output of FinisherSC as 'upgraded' assemblies. Next, we used tblastx to identify the contig in each upgraded assembly containing the best match to each of the 41 protein-coding genes in the *Cycas* mitogenome (Chaw et al. 2008), which we retained as 'high-confidence' assemblies. Then, we used pairwise alignments from NUCmer (Kurtz et al. 2004) to break the three assemblies at major disagreements. The resulting contigs were put through the assembly reconciliation pipeline implemented in CISA v. 1.3 (Lin & Liao 2013) to re-align them into a single, final draft. After checking for evidence of circularity of individual contigs using dot plots, we evaluated the quality of the assembly by aligning the corrected reads using minimap2 (Li 2018) to the draft and visually inspected their congruency in IGV v. 2.4.14. (Thorvaldsdóttir et al. 2012). Finally, we used the partial order alignment graph approach implemented in Racon to re-call the consensus sequence from the minimap2 alignment (Vaser et al. 2017).

Genome annotation

We reused repeat libraries curated for the *P. abies* v. 1.0 assembly (Nystedt et al. 2013) as input for RepeatMasker v. 4.0.7. (Smit et al. 2013) to identify TEs including long retrotransposons (LTRs), DNA transposable elements, and other interspersed elements (LINEs and SINES). We additionally used RepeatModeler v. 1.0.8. to identify potential *de novo* repeats with significant similarity to the RepBase and Dfam databases (Smit et al. 2013). Direct and inverted repeats were identified with self *vs.* self blastn searches following Guo et al. (2016). Mitochondrial DNA of plastid origin (MIPTs) were identified following the methods of Guo et al. (2016) and shared mitochondrial-nuclear DNA following the methods of (Alverson, Rice, et al. 2011).

We used MAKER v. 3.01.2 to annotate protein-coding genes (Cantarel et al. 2008). Complex repeats identified by RepeatMasker and RepeatModeler were hard-masked prior to

annotation, whereas simple repeats were re-annotated and soft masked by MAKER. As empirical gene evidence, we used the transcriptomes of *P. abies*, *P. glauca*, *P. sitchensis*, *Pinus pinaster*, *Pinus sylvestris*, and *Pinus taeda* from the PLAZA 3.0 database (Proost et al. 2014) and all curated plant sequences (Swiss-Prot) from UniProt as protein evidence. This provided a total of 312,953 ESTs and 37,954 proteins for use as evidence alignments. Although we initially attempted to use the SNAP and AUGUSTUS *ab initio* gene predictors, we found the number of high-confidence genes was insufficient for training. Therefore, presented annotations are based on empirical evidence alone. Coding sequences of all known genes were manually curated to improve identification of reading-frames and gene structure based on sequence homology. Hypothetical proteins were compared to an RNA-Seq dataset obtained from needles (PRJEB26398, Schneider et al., in preparation), in which transcripts were extracted using a ribo-minus and subjected to *de novo* transcriptome assembly using Trinity v. 2.8.4 using default parameters (Grabherr et al. 2011). The *de novo* reconstructed transcripts were aligned to the *P. abies* genome v. 1.0 retrieved from ConGenIE.org (Sundell et al. 2015) using the GMAP v. 2015.11.20 (Wu & Watanabe 2005). The alignment coordinates were intersected with the ab-initio prediction to validate the predicted hypothetical proteins using an ad-hoc R script.

Identification of repeat-mediated recombination and rearrangements

For each inverted repeat pair, we extracted the ± 2,000 bp single-copy flanking regions and artificially constructed their recombination products for use as an alternative genome reference (Day & Madesis 2007). We used minimap2 to map the enriched PacBio reads against these four sequences, with the expectation that reads spanning the repeat and flanking regions of the alternative configurations with robust mapping quality (MQ > 50) represent actual structural variations present within the sequenced individual tree (e.g. Park et al. 2014; Skippington et al. 2015; Cole et al. 2018; Dong et al. 2018).

We aligned the mitogenomes of *P. abies* and *P. glauca* using the rearrangement-aware progressiveMAUVE aligner (Darling et al. 2010), which identifies locally-collinear blocks (LCBs) internally free of recombination and reorders them against a selected genome. Then, we used GRIMM 2.01 (Tesler 2002) to infer a minimal, optimum rearrangement history, assuming signed undirected chromosomes. Apparent rearrangements introduced by the draft state of the genomes were corrected following Muñoz & Sankoff (2010) and Cole et al. (2018). Shared sequence between *P. abies* and *P. glauca* was estimated using blastn and the same parameters as

Guo et al. (2016) for consistency. To put the re-arrangement rates inferred in *Picea* into a broader phylogenetic context, we re-aligned and estimated minimum numbers of rearrangements from the species pairs in Guo et al. (2016) with similar levels of divergence (Table S6).

We searched manuscripts associated with all 127 tracheophyte mitogenomes in the NCBI Genome resource (accessed March 11, 2019) for estimations of recombination rates. In addition, we exhaustively searched Google Scholar for 'plant mitochondrial genomes' for publications since 2011, the year of the last extensive review of plant mitogenome recombination (Alverson, Zhuo, et al. 2011). To be included in our analysis, we required 1) sequences with high-throughput sequencing at a depth of coverage sufficient to allow detection of AGCs comprising ≥ 1.6% of the read pool, 2) repeat-by-repeat recombination rates inferred from mapping statistics or alignment rates reported in tables, or sufficiently detailed figures to allow precise interpolation from vectorized figures using Inkscape v. 0.91 (e.g. from Sloan et al. 2012). Wherever possible, we limited the analyses to repeats ≥ 50 bp with ≥ 80% identity. Relevant analytical details for each included study are summarized in Table S5.

Comparative analysis of gymnosperm mitogenomes

We downloaded the mitogenomes of *Amborella trichopoda, Cycas taitungensis, Ginkgo biloba, Welwitschia mirabilis, P. glauca,* and *Pinus taeda* from Genbank to compare substitution rates, gene and repeat content, and genomic structure. For analyses of nucleotide substitution rates, we also used the previously-sequenced mitogenome coding sequences of *Gnetum gnemon*. *Pinus sylvestris,* and *Araucaria heterophylla* from NCBI Genbank. Given the draft state of the *P. glauca* mitogenome, we retained only contigs with conserved mitochondrial genes, which resulted in a 5.2 Mb assembly. We re-annotated repeats and intergenome sequence transfers as described for *P. abies* to ensure consistent methodology across genomes.

Nucleotide substitution rates were estimated from the 41 protein-coding genes in Pinaceae. Coding sequences were extracted, aligned with MUSCLE v. 3.8.42 (Edgar 2004), and manually verified to ensure correct reading frames and complete codons. RNA editing sites were predicted using the PREP-mt webserver (Mower 2005) using a cutoff value of 0.2 as in Guo et al. (2016). Edited nucleotide sequences were re-aligned using the translation alignment option in Geneious v. 11.1.4 and poorly aligned blocks of codons were removed using Gblocks v. 0.91b webserver (Castresana 2000). First and second codon positions were extracted using DnaSP v. 6 (Rozas et al. 2017) and the maximum likelihood phylogeny of the concatenated alignment was

inferred using RAxML v. 8.2.12 (Stamatakis 2014) under the GTR-GAMMA model of nucleotide evolution. This phylogeny agreed with the prevailing consensus of gymnosperm evolution (Lu et al. 2014), so we estimated estimate branch lengths in units of synonymous (*d*S) and nonsynonymous (*d*N) substitution rates under the free-ratio branch model in PAML on this constrained topology (Yang 2007).

Intraspecific mitogenome variation in Picea abies

We selected two putatively ancient trees from (Kullman 2008) and collected newly-flushed buds. Buds were immediately placed in a solution comprising 10 mM MOPS, 5% (v/v) dimethylsulfoxide and 5% (w/v) glycerol at pH 7.3 and stored on dry ice and then at -80°C until mitochondria isolation. In brief, intact mitochondria were isolated using centrifugation and extraneous DNA was degraded using DNase, and then mitochondrial DNA was isolated using a gram-negative bacteria genomic DNA purification kit (Supplementary Methods 1). DNA library construction and PacBio RS II sequencing was performed at DUKE Center for Genomic and Computational Biology according to manufacturer's instructions.

PacBio sub-reads were checked for adapter contamination and then aligned to the whole *P. abies* v. 1.0 assembly containing the new *de novo* mitogenome using minimap2 (Li 2018). Scaffolds identified as mitochondrial-like by the SVM in the *P. abies* v. 1.0 assembly but that were not contained within the *de novo* assembly were left in place, as they may represent numts. Bases were called using GATK v. 3.8.0 Haplotype Caller in gvcf mode followed by joint-genotyping in `includeNonVariantSites` mode (Van der Auwera et al. 2013). As GATK does not assign confidence metrics to non-variant sites, we considered those covered by 10 to 35 reads to be represented. Sites with higher coverage represent unresolved repeats. Structural variants were called with Sniffles v. 1.0.11 using default filtering settings (Sedlazeck et al. 2018). Each structural variant was then visually validated in IGV v. 2.4.14. (Thorvaldsdóttir et al. 2012).

Acknowledgments

The authors acknowledge support from the National Genomics Infrastructure in Uppsala funded by Science for Life Laboratory, the Knut and Alice Wallenberg Foundation and the Swedish Research Council, and SNIC/Uppsala Multidisciplinary Center for Advanced Computational Science for assistance with massively parallel sequencing and access to the UPPMAX computational infrastructure, and the Danish Council for Independent Research – Natural Science (to IMM). NRS is supported by the Trees and Crops for the Future (TC4F) project.

References

Alexeyev M, Shokolenko I, Wilson G, LeDoux S. 2013. The maintenance of mitochondrial DNA integrity – critical analysis and update. Cold Spring Harb. Perspect. Biol. 5:a01264. doi: 10.1101/cshperspect.a012641

Alverson AJ et al. 2010. Insights into the evolution of mitochondrial genome size from complete sequences of *Citrullus lanatus* and *Cucurbita pepo* (Cucurbitaceae). Mol. Biol. Evol. 27:1436–1448. doi: 10.1093/molbev/msq029.

Alverson AJ, Rice DW, Dickinson S, Barry K, Palmer JD. 2011. Origins and recombination of the bacterial-sized multichromosomal mitochondrial genome of cucumber. Plant Cell. 23:2499–2513. doi: 10.1105/tpc.111.087189.

Alverson AJ, Zhuo S, Rice DW, Sloan DB, Palmer JD. 2011. The mitochondrial genome of the legume *Vigna radiata* and the analysis of recombination across short mitochondrial repeats. PLoS One. 6:e16404. doi: 10.1371/journal.pone.0016404.

André C, Levy A, Walbot V. 1992. Small repeated sequences and the structure of plant mitochondrial genomes. Trends Genet. 8:128–132. doi: 10.1016/0168-9525(92)90370-J.

Arrieta-Montiel M et al. 2001. Tracing evolutionary and developmental implications of mitochondrial stoichiometric shifting in the common bean. Genetics. 158:851–864.

Arrieta-Montiel MP, Mackenzie SA. 2011. Plant mitochondrial genomes and recombination. In: Kempken F (ed). Plant Mitochondria. Advances in Plant Biology, Vol 1. Springer: New York City pp. 65–82. doi: 10.1007/978-0-387-89781-3_3.

Van der Auwera GA et al. 2013. From fastQ data to high-confidence variant calls: the genome analysis toolkit best practices pipeline. Curr. Protoc. Bioinforma. 43: 11.10.1-11.10.33. doi: 10.1002/0471250953.bi1110s43.

Burger G, Gray MW, Franz Lang B. 2003. Mitochondrial genomes: anything goes. Trends Genet. 19:709–716. doi: 10.1016/j.tig.2003.10.012.

Buschiazzo E, Ritland C, Bohlmann J, Ritland K. 2012. Slow but not low: genomic comparisons reveal slower evolutionary rate and higher dN/dS in conifers compared to angiosperms. BMC Evol. Biol. 12:8. doi: 10.1186/1471-2148-12-8.

Cantarel BL et al. 2008. MAKER: an easy-to-use annotation pipeline designed for emerging model organism genomes. Genome Res. 18:188–196. doi: 10.1101/gr.6743907.

Castresana J. 2000. Selection of conserved blocks from multiple alignments for their use in phylogenetic analysis. Mol. Biol. Evol. 17:540–552. doi: 10.1093/oxfordjournals.molbev.a026334.

Chaw SM et al. 2008. The mitochondrial genome of the gymnosperm *Cycas taitungensis* contains a novel family of short interspersed elements, Bpu sequences, and abundant RNA editing sites. Mol. Biol. Evol. 25:603–615. doi: 10.1093/molbev/msn009.

Chen J et al. 2012. Sequencing of the needle transcriptome from Norway spruce (*Picea abies* Karst L.) reveals lower substitution rates, but similar selective constraints in gymnosperms and angiosperms. BMC Genomics. 13:589. doi: 10.1186/1471-2164-13-589.

Cho Y, Mower JP, Qiu Y-L, Palmer JD. 2004. Mitochondrial substitution rates are extraordinarily elevated and variable in a genus of flowering plants. Proc. Natl. Acad. Sci. U. S. A. 101:17741–17746. doi: 10.1073/pnas.0408302101.

Cole LW, Guo W, Mower JP, Palmer JD. 2018. High and variable rates of repeat-mediated mitochondrial genome rearrangement in a genus of plants. Mol. Biol. Evol. 35:2773–2785. doi: 10.1093/molbev/msy176.

Darling AE, Mau B, Perna NT. 2010. progressiveMauve: Multiple genome alignment with gene gain, loss and rearrangement. PLoS One. 5:e11147. doi: 10.1371/journal.pone.0011147.

Davila JI et al. 2011. Double-strand break repair processes drive evolution of the mitochondrial genome in *Arabidopsis*. BMC Biol. 9:64. doi: 10.1186/1741-7007-9-64.

Day A, Madesis P. 2007. DNA replication, recombination, and repair in plastids. In: Bock R (ed). Cell and Molecular Biology of Plastids. Springer: Berlin, Heidelberg pp. 65–119. doi: 10.1007/4735_2007_0231.

Eldfell, Y. 2018. Identifying mitochondrial genomes in draft whole-genome shotgun assemblies of six gymnosperm species. Bachelor's thesis. Stockholm University, Stockholm, Sweden.

Dong S et al. 2018. The complete mitochondrial genome of the early flowering plant *Nymphaea colorata* is highly repetitive with low recombination. BMC Genomics. 19:614. doi: 10.1186/s12864-018-4991-4.

Edgar RC. 2004. MUSCLE: multiple sequence alignment with high accuracy and high throughput. Nucleic Acids Res. 32:1792–1797. doi: 10.1093/nar/gkh340.

Ehrenmann F et al. 2015. Evidence of intense chromosomal shuffling during conifer evolution. Genome Biol. Evol. 7:2799–2809. doi: 10.1093/gbe/evv185.

Feng S et al. 2018. Trans-lineage polymorphism and nonbifurcating diversification of the genus *Picea*. New Phytol. 222:576-587. doi: 10.1111/nph.15590.

Giordano F et al. 2017. *De novo* yeast genome assemblies from MinION, PacBio and MiSeq platforms. Sci. Rep. 7:3935. doi: 10.1038/s41598-017-03996-z.

Goremykin V V, Lockhart PJ, Viola R, Velasco R. 2012. The mitochondrial genome of *Malus*

domestica and the import-driven hypothesis of mitochondrial genome expansion in seed plants. Plant J. 71:615–626. doi: 10.1111/j.1365-313X.2012.05014.x.

Grabherr MG et al. 2011. Full-length transcriptome assembly from RNA-Seq data without a reference genome. Nat. Biotechnol. 29:644. doi: 10.1038/nbt.1883.

Gray MW. 2014. The Pre-Endosymbiont Hypothesis: A new perspective on the origin and evolution of mitochondria. Cold Spring Harb. Perspect. Biol. 6:a016097. doi: 10.1101/cshperspect.a016097 .

Gray MW, Burger G, Lang BF. 1999. Mitochondrial Evolution. Science. 283:1476–1481. doi: 10.1126/science.283.5407.1476.

Gualberto JM, Newton KJ. 2017. Plant mitochondrial genomes: dynamics and mechanisms of mutation. Annu. Rev. Plant Biol. 68:225–252. doi: 10.1146/annurev-arplant-043015-112232.

Guo W et al. 2016. *Ginkgo* and *Welwitschia* mitogenomes reveal extreme contrasts in gymnosperm mitochondrial evolution. Mol. Biol. Evol. 33:1448–1460. doi: 10.1093/molbev/msw024.

Iorizzo M et al. 2012. *De novo* assembly of the carrot mitochondrial genome using next generation sequencing of whole genomic DNA provides first evidence of DNA transfer into an angiosperm plastid genome. BMC Plant Biol. 12:61. doi: 10.1186/1471-2229-12-61.

Jackman SD et al. 2015. Organellar genomes of white spruce (*Picea glauca*): Assembly and Annotation. Genome Biol. Evol. 8:29–41. doi: 10.1093/gbe/evv244.

Jayakumar V, Sakakibara Y. 2017. Comprehensive evaluation of non-hybrid genome assembly tools for third-generation PacBio long-read sequence data. Brief. Bioinform. 1–11. doi: 10.1093/bib/bbx147.

Joachims T. 1998. Making large-scale support vector machine learning practical. In: Schölkopf B, Burges C, Smola A. (eds). Advances in Kernel Methods: Support Vector machines. MIT Press: Cambridge (Massachusetts) pp. 169-184.

Knoop V et al. 1996. *copia*-, *gypsy*-, and LINE-Like retrotransposon fragments in the mitochondrial genome of *Arabidopsis thaliana*. Genetics. 142:579–585.

Koren S et al. 2017. Canu: scalable and accurate long-read assembly via adaptive k-mer weighting and repeat separation. Genome Res. 27:722–736. doi: 10.1101/gr.215087.116 .

Krutovsky K V, Troggio M, Brown GR, Jermstad KD, Neale DB. 2004. Comparative mapping in the Pinaceae. Genetics. 168:447–461. doi: 10.1534/genetics.104.028381.

Kullman L. 2008. Early postglacial appearance of tree species in northern Scandinavia: review and perspective. Quat. Sci. Rev. 27:2467–2472. doi: 10.1016/j.quascirev.2008.09.004.

Kullman L. 2001. Immigration of *Picea abies* into north-central Sweden. New evidence of regional expansion and tree-limit evolution. Nord. J. Bot. 21:39–54. doi: 10.1111/j.1756-1051.2001.tb01337.x.

Kurtz S et al. 2004. Versatile and open software for comparing large genomes. Genome Biol. 5:R12. doi: 10.1186/gb-2004-5-2-r12.

Lam K-K, Tse D, LaButti K, Khalak A. 2015. FinisherSC: a repeat-aware tool for upgrading *de novo* assembly using long reads. Bioinformatics. 31:3207–3209. doi: 10.1093/bioinformatics/btv280.

Lanfear R. 2018. Do plants have a segregated germline? PLoS Biol. 16:e2005439. doi: 10.1371/journal.pbio.2005439.

Leslie AB et al. 2018. An overview of extant conifer evolution from the perspective of the fossil record. Am. J. Bot. 105:1531–1544. doi: 10.1002/ajb2.1143.

Li H. 2018. Minimap2: pairwise alignment for nucleotide sequences. Bioinformatics. 34:3094–3100. doi: 10.1093/bioinformatics/bty191.

Lin S-H, Liao Y-C. 2013. CISA: Contig integrator for sequence assembly of bacterial genomes. PLoS One. 8:e60843. doi: 10.1371/journal.pone.0060843.

Lonsdale DM, Hodge TP, Fauron CM. 1984. The physical map and organisation of the mitochondrial genome from the fertile cytoplasm of maize. Nucleic Acids Res. 12:9249–9261.

Lu Y, Ran J-H, Guo D-M, Yang Z-Y, Wang X-Q. 2014. Phylogeny and divergence times of gymnosperms inferred from single-copy nuclear genes. PLoS One. 9:e107679. doi: 10.1371/journal.pone.0107679.

Maréchal A, Brisson N. 2010. Recombination and the maintenance of plant organelle genome stability. New Phytol. 186:299–317. doi: 10.1111/j.1469-8137.2010.03195.x.

Miller-Messmer M et al. 2012. RecA-dependent DNA repair results in increased heteroplasmy of the *Arabidopsis* mitochondrial genome. Plant Physiol. 159:211–226. doi: 10.1104/pp.112.194720.

Mower JP. 2005. PREP-Mt: predictive RNA editor for plant mitochondrial genes. BMC Bioinformatics. 6:96. doi: 10.1186/1471-2105-6-96.

Mower JP, Floro ER, Case AL, Willis JH. 2012. Evidence against equimolarity of large repeat arrangements and a predominant master circle structure of the mitochondrial genome from a monkeyflower (*Mimulus guttatus*) mineage with cryptic CMS. Genome Biol. Evol. 4:670–686. doi: 10.1093/gbe/evs042.

Mower JP, Sloan DB, Alverson AJ. 2012. Plant mitochondrial genome diversity: the genomics revolution. In: Wendel J, Greilhuber J, Dolezel J, Leitch I (eds). Plant Genome Diversity, Vol 1. Springer: Vienna, pp. 123–144. doi: 10.1007/978-3-7091-1130-7_9.

Mower JP, Touzet P, Gummow JS, Delph LF, Palmer JD. 2007. Extensive variation in synonymous substitution rates in mitochondrial genes of seed plants. BMC Evol. Biol. 7:135. doi: 10.1186/1471-2148-7-135.

Muñoz A, Sankoff D. 2010. Rearrangement phylogeny of genomes in contig form. IEEE/ACM Trans. Comput. Biol. Bioinforma. 7:579–587. doi: 10.1109/TCBB.2010.66.

Naito K, Kaga A, Tomooka N, Kawase M. 2013. *De novo* assembly of the complete organelle genome sequences of azuki bean (*Vigna angularis*) using next-generation sequencers. Breed. Sci. 63:176–182. doi: 10.1270/jsbbs.63.176.

Nystedt B et al. 2013. The Norway spruce genome sequence and conifer genome evolution. Nature. 497:579–84. doi: 10.1038/nature12211.

Palmer JD, Herbon LA. 1988. Plant mitochondrial DNA evolves rapidly in structure, but slowly in sequence. J. Mol. Evol. 28:87–97.

Palmer JD, Shields CR. 1984. Tripartite structure of the *Brassica campestris* mitochondrial genome. Nature. 307:437–440. doi: 10.1038/307437a0.

Park S et al. 2014. Complete sequences of organelle genomes from the medicinal plant *Rhazya stricta* (Apocynaceae) and contrasting patterns of mitochondrial genome evolution across asterids. BMC Genomics. 15:405. doi: 10.1186/1471-2164-15-405.

Pavy N et al. 2012. A spruce gene map infers ancient plant genome reshuffling and subsequent slow evolution in the gymnosperm lineage leading to extant conifers. BMC Biol. 10:84. doi: 10.1186/1741-7007-10-84.

Pelgas B et al. 2006. Comparative genome mapping among *Picea glauca*, *P. mariana* x *P. rubens* and *P. abies*, and correspondence with other Pinaceae. Theor. Appl. Genet. 113:1371–1393. doi: 10.1007/s00122-006-0354-7.

Pinard D, Myburg AA, Mizrachi E. 2019. The plastid and mitochondrial genomes of *Eucalyptus grandis*. BMC Genomics. 20:132. doi: 10.1186/s12864-019-5444-4.

Proost S et al. 2014. PLAZA 3.0: an access point for plant comparative genomics. Nucleic Acids Res. 43:D974–D981. doi: 10.1093/nar/gku986.

Rice DW et al. 2013. Horizontal transfer of entire genomes via mitochondrial fusion in the angiosperm *Amborella*. Science 342:1468–1473. doi: 10.1126/science.1246275.

Richardson AO, Rice DW, Young GJ, Alverson AJ, Palmer JD. 2013. The “fossilized” mitochondrial genome of *Liriodendron tulipifera*: ancestral gene content and order, ancestral editing sites, and extraordinarily low mutation rate. BMC Biol. 11:29. doi: 10.1186/1741-7007-11-29.

Rodríguez-Moreno L et al. 2011. Determination of the melon chloroplast and mitochondrial genome sequences reveals that the largest reported mitochondrial genome in plants contains a significant amount of DNA having a nuclear origin. BMC Genomics. 12:424. doi: 10.1186/1471-2164-12-424.

Rozas J et al. 2017. DnaSP 6: DNA sequence polymorphism analysis of large data sets. Mol. Biol. Evol. 34:3299–3302. doi: 10.1093/molbev/msx248.

Saladin B et al. 2017. Fossils matter: improved estimates of divergence times in *Pinus* reveal older diversification. BMC Evol. Biol. 17:95. doi: 10.1186/s12862-017-0941-z.

Sedlazeck FJ et al. 2018. Accurate detection of complex structural variations using single-molecule sequencing. Nat. Methods. 15:461–468. doi: 10.1038/s41592-018-0001-7.

Shedge V, Arrieta-Montiel M, Christensen AC, Mackenzie SA. 2007. Plant mitochondrial recombination surveillance requires unusual *RecA* and *MutS* homologs. Plant Cell. 19:1251–1264. doi: 10.1105/tpc.106.048355.

Shedge V, Davila J, Arrieta-Montiel MP, Mohammed S, Mackenzie SA. 2010. Extensive rearrangement of the *Arabidopsis* mitochondrial genome elicits cellular conditions for thermotolerance. Plant Physiol. 152:1960–1970. doi: 10.1104/pp.109.152827.

Skippington E, Barkman TJ, Rice DW, Palmer JD. 2015. Miniaturized mitogenome of the parasitic plant *Viscum scurruloideum* is extremely divergent and dynamic and has lost all nad genes. Proc. Natl. Acad. Sci. 112:E3515–E3524. doi: 10.1073/pnas.1504491112.

Sloan DB. 2013. One ring to rule them all? Genome sequencing provides new insights into the 'master circle' model of plant mitochondrial DNA structure. New Phytol. 200:978–985. doi: 10.1111/nph.12395.

Sloan DB et al. 2012. Rapid evolution of enormous, multichromosomal genomes in flowering plant mitochondria with exceptionally high mutation rates. PLOS Biol. 10:e1001241. doi: journal.pbio.1001241.

Smit AFA, Hubley R, Green, P. 2013. RepeatMasker Open-4.0. <http://www.repeatmasker.org>.

Stamatakis A. 2014. RAxML version 8: a tool for phylogenetic analysis and post-analysis of large phylogenies. Bioinformatics. 2010–2011. doi: 10.1093/bioinformatics/btu033.

Sullivan AR, Schiffthaler B, Thompson SL, Street NR, Wang X-R. 2017. Interspecific plastome recombination reflects ancient reticulate evolution in *Picea* (Pinaceae). Mol. Biol. Evol. 34:1689–1701. doi: 10.1093/molbev/msx111.

Sundell D et al. 2015. The Plant Genome Integrative Explorer resource: PlantGenIE.org. New Phytol. 208:1149–1156. doi: 10.1111/nph.13557.

Tesler G. 2002. GRIMM: genome rearrangements web server. Bioinformatics. 18:492–493. doi: 10.1093/bioinformatics/18.3.492.

Thorvaldsdóttir H, Robinson JT, Mesirov JP. 2012. Integrative Genomics Viewer (IGV): high-performance genomics data visualization and exploration. Brief. Bioinform. 14:178–192. doi: 10.1093/bib/bbs017.

Tiley GP, Burleigh JG. 2015. The relationship of recombination rate, genome structure, and patterns of molecular evolution across angiosperms. BMC Evol. Biol. 15:194. doi: 10.1186/s12862-015-0473-3.

Vaser R, Sovic I, Nagarajan N, Sikic M. 2017. Fast and accurate *de novo* genome assembly from long uncorrected reads. Genome Res. 27:737-746. doi: 10.1101/gr.214270.116

Wallet C et al. 2015. The RECG1 DNA translocase is a key factor in recombination surveillance, repair, and segregation of the mitochondrial DNA in *Arabidopsis*. Plant Cell. 27:2907–2925. doi: 10.1105/tpc.15.00680.

Wang B, Wang X-R. 2014. Mitochondrial DNA capture and divergence in *Pinus* provide new insights into the evolution of the genus. Mol. Phylogenet. Evol. 80:20–30. doi: 10.1016/j.ympev.2014.07.014.

Wang S et al. 2018. Assembly of a complete mitogenome of *Chrysanthemum nankingense* using Oxford Nanopore long reads and the diversity and evolution of Asteraceae mitogenomes. Genes.

9:547. doi: 10.3390/genes9110547.

Ward BL, Anderson RS, Bendich AJ. 1981. The mitochondrial genome is large and variable in a family of plants (Cucurbitaceae). Cell. 25:793–803.

Woloszynska M. 2009. Heteroplasmy and stoichiometric complexity of plant mitochondrial genomes—though this be madness, yet there's method in't. J. Exp. Bot. 61:657–671. doi: 10.1093/jxb/erp361.

Wu TD, Watanabe CK. 2005. GMAP: a genomic mapping and alignment program for mRNA and EST sequences. Bioinformatics. 21:1859–1875. doi: 10.1093/bioinformatics/bti310.

Wynn EL, Christensen AC. 2019. Repeats of unusual size in plant mitochondrial genomes: identification, incidence and evolution. G3-Genes Genom. Genet. 9:549–559. doi: 10.1534/g3.118.200948.

Xiao C Le et al. 2017. MECAT: Fast mapping, error correction, and *de novo* assembly for single-molecule sequencing reads. Nat. Methods. 14:1072–1074. doi: 10.1038/nmeth.4432.

Yang Z. 2007. PAML 4: Phylogenetic analysis by maximum likelihood. Mol. Biol. Evol. 24:1586–1591. doi: 10.1093/molbev/msm088.

Zaegel V et al. 2006. The plant-specific ssDNA binding protein OSB1 Is involved in the stoichiometric transmission of mitochondrial DNA in *Arabidopsis*. Plant Cell. 18:3548–3563. doi: 10.1105/tpc.106.042028.